A time dependent propagator method for long mean free path transport of neutral particles in plasma processing reactors

Wen-yi Tan, Robert J. Hoekstra, and Mark J. Kushner[a)]
Department of Electrical and Computer Engineering, University of Illinois, 1406 W. Green Street, Urbana, Illinois 61801

(Received 5 October 1995; accepted for publication 18 December 1995)

Plasma etching reactors for microelectronics fabrication are moving towards operating at lower gas pressures (<10 mTorr). These pressures are sufficiently low that simulations using continuum modeling techniques may not be strictly applicable. A time dependent kinetic method based on the use of a transition matrix (propagator) has been developed and applied to the calculation of long mean free path transport of neutral species in an inductively coupled plasma (ICP) etching reactor. The propagator $P(\mathbf{r},\mathbf{r}')$ provides the probability that particles originating at location $\mathbf{r}'$ will have their next collision at location $\mathbf{r}$. The species densities obtained from this model are compared with results from fluid and Monte Carlo simulations for various mean free paths. We find that the propagator model is valid when the mean free path of the particles is larger than the numerical cell dimension and that fluid methods for long mean free path transport can be corrected to obtain the Monte Carlo or propagator results by employing an effective diffusion coefficient. Time dependent results are generating by employing a retarded time in which flights of particles beginning at past times from remote locations are used to determine the present value of the local collision frequency. Self-consistent neutral densities in ICP discharges for various pressures are obtained by employing the propagator model in a hybrid ICP model. © *1996 American Institute of Physics.* [S0021-8979(96)05407-1]

I. INTRODUCTION

Plasma processing for submicron semiconductor fabrication is moving towards using reactors operating at lower gas pressures and higher plasma densities. Examples of these devices are inductively coupled plasma (ICP) and electron cyclotron resonance (ECR) etching reactors.[1–6] In many instances, the mean free path of neutral atoms or radicals is commensurate to the dimensions of the reactor at the pressure of interest [1–20 mTorr, Knudsen number (Kn)>0.1]. The use of fluid continuity and momentum equations to calculate the density of neutral species may therefore not be strictly valid. Monte Carlo (MC) simulations are typically used to describe long mean free path transport of neutral species under these conditions. The MC method, which tracks the trajectories of individual neutral pseudoparticles under the influence of scattering forces, in many cases provides the most accurate results for neutral transport. For example, direct simulation Monte Carlo (DSMC) (Ref. 7) and conventional MC methods[8,9] have been employed to investigate charged and neutral transport in ICP reactors at low pressures (<5–10 mTorr) in two dimensions. Particle in cell (PIC) simulations employing MC methods have similarly been used for two-dimensional simulations of ICP and reactive ion etching (RIE) discharges.[10] PIC and MC simulations are, however, computationally intensive and may not be suitable for conditions where there is a large dynamic range in species densities in multicomponent and reactive systems.

Recently, a new method for calculating long mean free path transport has been demonstrated by Harvey *et al.* and has been applied to a low pressure ECR etching system.[11,12] This method is based the use of a ''transition matrix.'' or ''propagator,'' for each neutral species having an arbitrary mean free path λ.[13,14] The propagator describes the probability that a particle, having suffered a collision or been produced at a remote location, will have its next collision at the location of interest. The propagator is employed during the simulation of species densities by providing the fractional density which is transported from one computational cell to another. After the propagator is created, it can be repeatedly used to calculate the steady state density of that species if the production rates are known. Unlike MC simulations, the propagator method can be nonstatistical, and therefore has the potential of being more accurate. Since the propagator method does not track individual particles, it also has the potential to be computationally faster.

In this study, we extended the previous implementation of the propagator method to a time dependent form by employing a retarded time. In doing so, the finite flight times of density elements from distant locations are accounted for. For demonstration purposes, we implemented the time dependent propagator (TDP) as the neutral transport module in a hybrid model for ICP reactors.[8,9] In doing so, the TDP method is compared to the results of fluid and MC calculations over a range of mean free paths. The TDP model is described in Sec. II followed by a discussion of validation of the TDP in Sec. III. The implementation of the TDP method in the hybrid model for an ICP reactor is discussed in Sec. IV, followed by concluding remarks in Sec. V.

II. DESCRIPTION OF THE MODEL

A. The time dependent propagator method

To implement the TDP method, a probability matrix (the ''propagator'') $P(\mathbf{r},\mathbf{r}')$ for each neutral species with a given

a)Author to whom correspondence should be addressed; Electronic mail: mjk@uiuc.edu

mean free path λ must be first generated. The propagator describes the probability per unit volume that a particle, which had its last collision or originates at location $\mathbf{r}'$, will have its next collision at location $\mathbf{r}$.[1–14] In general, if we assume that collisions are isotropic, then

$$P(\mathbf{r},\mathbf{r}')=\frac{\exp\left(\frac{-|\mathbf{r}-\mathbf{r}'|}{\lambda}\right)}{4\pi|\mathbf{r}-\mathbf{r}'|^2\int\frac{\exp\left(\frac{-|\mathbf{r}-\mathbf{r}''|}{\lambda}\right)d^3\mathbf{r}''}{4\pi|\mathbf{r}-\mathbf{r}''|^2}}. \tag{1}$$

In this expression, we evaluate the probability of arrival of spherical ''shells'' of isotropically scattered atoms at the location of interest. Although $P(\mathbf{r},\mathbf{r}')$ can be evaluated analytically, in complex geometries where surface reactions may occur, it is convenient to evaluate $P(\mathbf{r},\mathbf{r}')$ using MC methods, and in this work we have used the latter method. Note that the nonstatistical implementation of the propagator is independent of the method of construction of the propagator.

To construct $P(\mathbf{r},\mathbf{r}')$ using MC methods, particles originating in the computational cell $\mathbf{r}'$ are launched using a spatially uniform distribution and a randomly selected isotropic velocity. The flight distance of the particle is chosen as $\delta=-\lambda\ln(r)$ where r is a random number distributed (0,1). The trajectory of the particle is integrated, accounting for interception of boundaries, for a distance δ, and the computational cell it occupies at the end of its flight, $\mathbf{r}$, is recorded. The number of particles that arrive in each final cell is divided by the number of particles injected from the initial cell to determine the transition probability. Since the particles may have sticking coefficients other than unity or react to form other species at boundaries, it necessary to construct propagator entries for flight paths which both intercept and originate from boundaries. In practice, $P(\mathbf{r},\mathbf{r}')$ is constructed separately from the actual transport calculation, and stored for later use. To save computer memory, we defined a horizon beyond which we ignore scattering contributions to the local cell. The radius of the horizon is typically $\geqslant 3\lambda$.

The propagator $P(\mathbf{r},\mathbf{r}')$ holds the transport properties for each species, and so the rate at which particles arrive at $\mathbf{r}$ ($\mathrm{cm}^{-3}\,\mathrm{s}^{-1}$) is

$$R(\mathbf{r},t)=\int_\nu P(\mathbf{r},\mathbf{r}')N(\mathbf{r}',t')\,\nu_c(\mathbf{r}')d^3r'-\nu_c(\mathbf{r})N(\mathbf{r},t)+S(\mathbf{r},t)+\left(\frac{\partial N(\mathbf{r},t)}{\partial t}\right)_s. \tag{2}$$

In Eq. (2). $S(\mathbf{r},t)$ is the net source function for the species resulting from electron impact and heavy particle collisions, and ν_c is the momentum transfer collision frequency of the species, t' is time of the scattering event at $\mathbf{r}'$, and is discussed below. For our purposes, we assumed isotropic collisions and define $\nu_c=\lambda/v_t$, where v_t is the thermal speed of the atom or molecule. The first term on the right hand side of Eq. (2) accounts for the arrival of particles at $\mathbf{r}$ due to flights of particles which were last scattered at $\mathbf{r}'$. The second term accounts for the outscatter of particles from $\mathbf{r}$ to other locations. The last term is for contributions to the local density which comes from particles which scatter off of surfaces. This contribution is

$$\left(\frac{dN(\mathbf{r},t)}{dt}\right)_s=\oint_{\text{surface}}P(\mathbf{r},\mathbf{r}')[R(\mathbf{r}',t')]_0\times[1-\alpha(\mathbf{r}')]d\mathbf{r}', \tag{3}$$

where $\alpha(\mathbf{r}')$ is the sticking coefficient for the neutral species at surface cell $\mathbf{r}'$. $[R(\mathbf{r}',t')]_0$ represents the arrival flux of species at the surface. In the quasisteady state one may set $t'=t$. The net arrival of particles $R(\mathbf{r},t)=0$ since the inscatter and formation rates equals the outscatter rates, and Eq. (2) may be iterated to obtain $N(\mathbf{r},t)$. Note that the density in Eq. (2) is a collision density which does not necessarily account for the density of particles in flight between collisions. This issue will be discussed later in this section.

If time dependent densities are desired, that is $R(\mathbf{r},t)\neq 0$, then one must account for the finite flight time between a particle's last scattering event at $\mathbf{r}'$ and its arrival at $\mathbf{r}$. This is accomplished by setting $t'=t_r$, where t_r is the retarded time, or past time, at which the particle began its flight. This retarded time is

$$t_r=t-\frac{|\mathbf{r}-\mathbf{r}'|}{v_t}. \tag{4}$$

From a computational standpoint, the retarded time is implemented by saving a past history of particle densities in a first-in-first-out (FIFO) stack. The species density at a specific retarded time is then obtained by interpolating the past history of densities at a given location. Typically, we save past histories of densities for sufficient times for particles to cross the ''event horizon,'' or travel a distance of $\sim 3\lambda$.

The neutral density obtained by the propagator model [Eq. (2)] is based on the rates of collision and therefore can be thought of as a collision density. One should interpret the density as providing a collision rate $N(\mathbf{r},t)\nu_c$. That density may not, however, be the value which will be experimentally observed at low pressures by, for example, laser induced fluorescence (LIF) measurements. Consider the situation where the neutral atom mean free path is very large compared to the wall separation ($\mathrm{Kn}\gg 1$). These atoms will simply ''bounce'' back and forth between the cavity walls while suffering few gas phase collisions. The propagator model just described would predict that the density is concentrated at the walls because that is where the collisions occur. Neutral density would still be experimentally observed inside the reactor during the particle flights between collisions. Therefore, the collisional density obtained by the propagator method must be corrected.[12] This is performed by using a second transition matrix, $T(\mathbf{r},\mathbf{r}')$, which denotes the total time a fluid element launched from cell r spends in cell $\mathbf{r}'$. Similar to the propagator matrix P, $T(\mathbf{r},\mathbf{r}')$ can also be calculated by using the MC method and stored for later use. In this study, $T(\mathbf{r},\mathbf{r}')$ is defined as

$$T(\mathbf{r},\mathbf{r}')=\frac{1}{N_p}\sum_{i=1}^{N_p}\frac{\int_{\mathbf{s}}\delta(\mathbf{s}-\mathbf{r}')\frac{d\mathbf{s}}{v}}{\int_{\mathbf{s}}\delta(\mathbf{s}-\mathbf{r}')d^3s}, \tag{5}$$

where N_p is the total number of particles launched from $\mathbf{r}$. The integral is over the path of the particle prior to having a collision from its launch point and v is the speed of the particle. With $T(\mathbf{r},\mathbf{r}')$ so determined, the collisional species density obtained from the TDP method can be corrected to generate the observed densities, N_0 by

$$N(\mathbf{r},t)_0 = \int N_{\mathrm{TDP}}(\mathbf{r}',t)\,\nu(\mathbf{r}')\,T(\mathbf{r}',\mathbf{r})\,d^3r'. \tag{6}$$

If the transport is sufficiently collisional, then $T(\mathbf{r},\mathbf{r}')$ is essentially a volume weighted collision time, and $N_0 \approx N_{\mathrm{TDP}}$.

In the following discussion, the mean free path is constant for a given set of operating conditions and the particles are monoenergetic. The propagator method can, however, be generalized to address spatially dependent mean free paths and energies. This generalization is discussed by Harvey *et al.* in Ref. 11.

B. Validation by comparison to fluid and Monte Carlo methods

We employed two different techniques to calculate the same densities to validate the time dependent propagator method. The first is a continuum fluid model where the densities are obtained from

$$\frac{dN(\mathbf{r},t)}{dt} = -\nabla\cdot[-D\nabla N(\mathbf{r},t)] + S(\mathbf{r},t). \tag{7}$$

In Eq. (7), D is the particle continuum diffusion coefficient, defined here as $D=\lambda v_t$. This partial differential equation, couched in finite difference form using the donor cell technique, was integrated as a function of time using a simple Runga–Kutta method. The boundary condition for particle fluxes at the wall is incorporated as a jump condition, $\phi_2=(1-\alpha)\phi_1$, where ϕ_1 is the flux exiting the boundary cell (assuming zero density on the walls) and ϕ_2 is the flux returning to the volume from the wall.

The second method used for validation of the TDP is a Monte Carlo simulation (MCS). Pseudoparticles were sourced from specified locations having thermal speeds with randomly selected directions. The weighting of an individual pseudoparticle was

$$W = \frac{1}{N_p}\int S(\mathbf{r})\,d^3r \ \ \mathrm{s}^{-1}, \tag{8}$$

where $S(\mathbf{r})$ [$\mathrm{cm}^{-3}\,\mathrm{s}^{-1}$] is the particle source function and N_p is the total number of pseudoparticles. The path length to the next collision was chosen as $\delta=-\lambda\ln(r)$, where r is a random number distributed (0,1). Collisions were assumed to be isotropic. Statistics were continually collected along the path the pseudoparticle, to yield a particle density $N(\mathbf{r})$.

$$N(\mathbf{r})\,d^3\mathbf{r} = \sum_i W_i \int \frac{\delta(\mathbf{r}-\mathbf{s})}{v_i}\,d\mathbf{s}. \tag{9}$$

C. The hybrid plasma equipment model

The TDP method was implemented as the neutral kinetic model in a simulation for plasma etching equipment. This simulation, called the hybrid plasma equipment model (HPEM), is a comprehensive model of the electromagnetic field, electron kinetics and plasma chemistry in a plasma etching reactor. The HPEM is discussed in detail in Refs. 8 and 9, and so will be only briefly described here. The two-dimensional HPEM is composed of a series of modules which are iterated to a converged solution. The electromagnetics module (EMM) generates inductively coupled electric and magnetic fields in the reactor. These fields are next used in the electron Monte Carlo simulation (EMCS) module. In the EMCS electron trajectories are followed for many rf cycles producing the electron energy distribution as a function of position and phase. These distributions are used to produce electron impact source functions for ion and neutral species which are transferred to the fluid kinetics simulation (FKS) module. In the FKS, continuity and momentum equations are solved for all neutral and charged particle densities, and Poisson's equation is solved for the electric potential. The plasma conductivity produced in the FKS is passed to the EMM, and the species densities and time dependent electrostatic potential are passed to the EMCS. The modules are iterated until cycle averaged plasma densities converge. Acceleration algorithms are used to speed the rate of convergence of the model.

The FKS module of the HPEM in Ref. 8 uses conventional fluid equations for species densities and momenta. As a result, long mean free path effects are not well represented. The TDP method described here was therefore incorporated into the HPEM as a kinetic transport module in the FKS. Due to the modular nature of the HPEM, this substitution was easily performed by replacing the subroutines which generated the time derivatives for species densities (the fluid continuity and momentum equations) with a subroutine incorporating Eqs. (2)–(6). No other changes were made to the HPEM.

III. VALIDATION

The time dependent propagator model was validated by comparing neutral particle densities obtained with the TDP with densities calculated with the fluid model and MCS. For purposes of demonstration, we have chosen to use an ICP etching reactor for our test geometry.[1–5] This system is used for low pressure ($<$10–20 mTorr) etching of semiconductor materials and metals for microelectronics fabrication. The particular ICP geometry of interest is shown in Fig. 1(a). The top coil dominantly produces an azimuthal electric field and power deposition which has a maximum in the plasma at approximately half the radius just under the dielectric roof. The low operating pressure results in dominantly diffusive or long mean free path transport which helps to homogenize the radical and ion fluxes prior to striking the substrate and wafer. Characteristics of this reactor are discussed in Refs. 1–5. The plasma zone dimensions are 17.8 cm in radius and 8 cm in height. The mesh was chosen to have a uniform grid size of $\Delta r=\Delta z=0.25$ cm over the plasma region.

For purposes of validation, in Sec. III we will simply specify the production rate of the neutral species as a function of position. Self-consistent results for ICP etching tools using the TDP method will be presented in Sec. IV. We used argon as the background gas and injected an excited Ar*

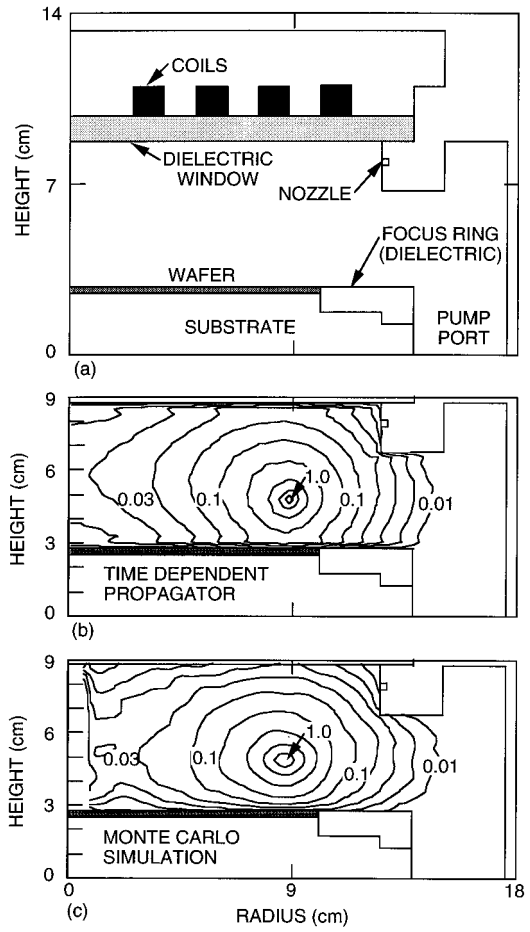

FIG. 1. Comparison between the TDP and MCS methods for long mean free path transport. (a) ICP geometry used in this study. The plasma is generated by a flat coil situated above a dielectric window. Steady state densities for Ar* obtained with the (a) TDP and (b) MCS methods for $\lambda=1.25$ cm. The contours are labeled with their fraction of the maximum value. The spatial distributions of the densities obtained with the TDP and MCS methods agree well.

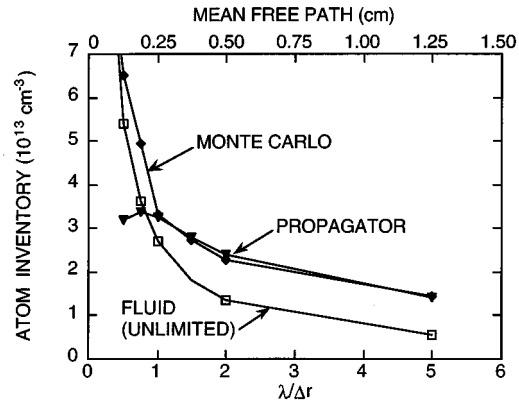

FIG. 2. Total inventory of Ar* atoms obtained with the TDP, MCS, and unlimited fluid methods as a function of mean free path (or $\lambda/\Delta r$). The TDP and MCS methods agree well for when $\lambda/\Delta r>1$. The unlimited fluid method over predicts loss for $\lambda/\Delta r>1$, and matches the MCS results for these conditions only for $\lambda/\Delta r<0.5$.

species, nominally Ar($4s$), at a single point located at approximately half the radius and the half height ($r=8.9$ cm, $z=4$ cm). The atom generation rate in that numerical cell was 1.0×10^{16} cm^{-3}s^{-1}. The neutral temperature was 500 °K. The gas pressure was varied to produce mean free paths for neutral–neutral collisions for Ar* of 0.125–1.25 cm ($\lambda=0.5$–$5.0\Delta r$), corresponding to gas pressures of 100–10 mTorr at 500 °K. These parameters were then used to generate the appropriate propagator matrix using the MC method. The numerical time step was 1 μs. The quenching probability of the excited state is unity and uniform on all surfaces unless stated otherwise.

The first validation of the TDP was performed by comparing the steady state densities of Ar* obtained with the TDP and MCS, and these densities are shown in Figs. 1(b) and 1(c). The quantitative agreement between the two methods is quite good accept near the axis where the MCS has poor statistics. Even though the boundary condition is that Ar* is quenched on the surfaces (equivalent to Ar*=0 on surfaces for a continuum model), the gas phase densities do not extrapolate to zero at the boundaries. This trend is characteristic of long mean free path transport.[7,11,12] The TDP has a small increase density in the last cell near the boundary which does not appear in the MCS. This is an artifact of using a coarse mesh when applying the transition matrix $T(\mathbf{r},\mathbf{r}')$ to convert from collision frequencies to real densities.

The TDP method was next validated by comparing steady state inventories of excited atoms obtained from the fluid model and MCS. These excited atom inventories (total density of Ar* in the reactor) are shown in Fig. 2. Atom inventories decrease with increasing λ due to the larger rate of loss afforded by the lower collision rate in the gas phase. The atom inventories obtained by the TDP and by fluid methods are only in close agreement when $\lambda\approx\Delta r$. For $\lambda<\Delta r$, the inventories predicted by the fluid method continue to increase in proportion to $1/\lambda$ to reflect the smaller rates of loss due by diffusion. The inventories predicted by the TDP method are nearly constant. For $\lambda>\Delta r$, the inventories predicted by the propagator model are larger than the fluid method. These phenomena might be explained as follows: when $\lambda/\Delta r>1$, the fluid method is technically not valid since the mean free path of the atoms is larger than the cell size. As a result, the excited atoms flow to the boundary and are lost on the walls too quickly. That is, the diffusion speed, $v_d=|D(\nabla N/N)|$, may exceed the thermal speed. When $\lambda/\Delta r<1$, the TDP is not applicable since particles scattering in cell $\mathbf{r}'$ will have their next collision in the same cell $\mathbf{r}'$. As a result, when $\lambda/\Delta r<1$ the propagator matrices for all mean free paths will be similar, and consequently the resulting densities will remain nearly constant. (This situation may be exacerbated by our use of an event horizon.) The only values of mean free path where *both* methods are simultaneously valid are $\lambda/\Delta r\approx1$.

The atom inventories obtained using the fluid method track the inventories generated using the MCS for $\lambda/\Delta r<0.5$ (all data are not shown in Fig. 2). The inventories generated using the TDP method track those from the MCS for $\lambda/\Delta r>1$. Assuming the MC method is valid for arbitrary mean free paths, one finds that the TDP is a meaningful method for calculating particle densities with the mean free path exceeds the dimension of the computational cell. For mean free paths

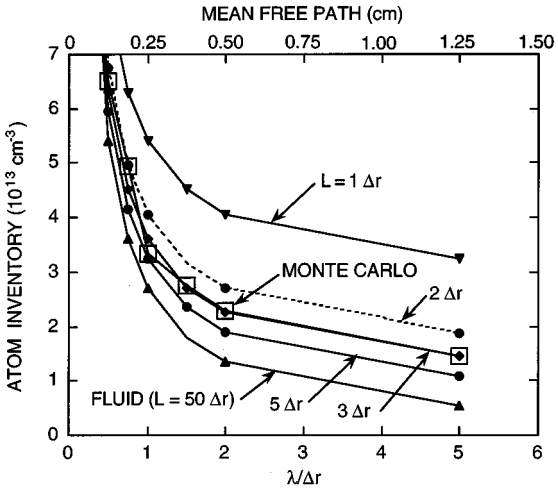

FIG. 3. Total inventory of Ar* atoms obtained with the MCS and fluid methods when the fluid diffusion flux is limited according to the diffusion length L. The fluid method agrees with the MCS over a long range of mean free paths for $L=3\Delta r$ which is small compared to the reactor size.

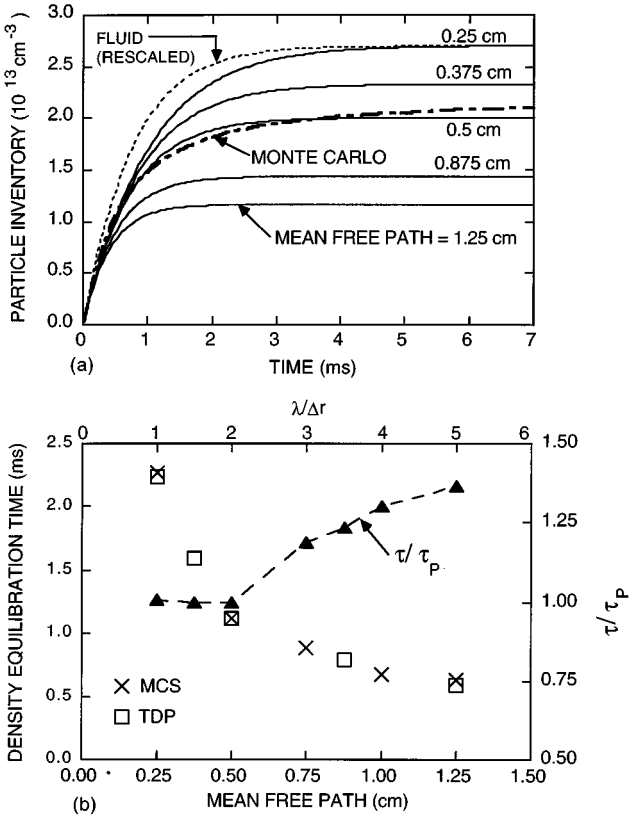

FIG. 4. Time dependent properties for total particle inventory. (a) Inventory as a function of time as obtained with the TDP for various mean free paths with comparisons to the MCS and fluid model. The magnitude of the fluid result has been rescaled. (b) Times at which the particle inventories obtained with the TDP and MCS equilibrate as a function of mean free path. We also show the actual equilibration time scaled by the equilibration time for continuum transport.

having shorter values, the TDP is unable to sufficiently resolve the problem.

The calculation of species densities using gradient driven (Fick's law) transport can be extended to lower pressures by preventing the effective diffusion length from exceeding the dimension of the vessel. Equivalently stated, the diffusion speed cannot exceed the thermal speed. This limit can be expressed as

$$D=\frac{v_t\lambda}{1+\dfrac{\lambda}{\Lambda}}, \tag{10}$$

where Λ is the effective diffusion length. As the pressure decreases and the mean free path λ increases, D approaches a constant value $D=v_t\Lambda$. For fundamental mode diffusion, Λ is a known function of the dimensions of the container. Otherwise, Λ may have a complex dependence on the shape of the container, distribution of the sources and sinks of the species in question, or depend on other thermodynamic quantities such as temperature. This technique is similar to flux limiting.[15]

To illustrate these dependencies, we parameterized Λ of Eq. (10) in the fluid equations to determine values which would extend our calculations to lower pressures. The conditions are the same as discussed above (a point source) and the resulting particle inventories are shown in Fig. 3. The fluid and MC results agree well for $\Lambda=3\Delta r$ for a wide range of mean free paths. The small value for Λ compared to the dimensions of the reactor is a consequence of the steep gradient in particle density resulting from the point source (as shown in Fig. 1). More distributed sources will result in a larger Λ.

The total inventories of excited atoms in the reactor as a function of time as obtained with the TDP are shown in Fig. 4(a). The mean free path was varied between 0.25 and 1.25 cm. Representative results from the MCS and fluid models are also shown. As expected, the densities come to equilibrium at shorter times for lower pressures where the diffusion speed is higher. The comparison with the fluid calculation (rescaled in magnitude to match the TDP) is made at the smallest mean free path where $\lambda=\Delta r$, the point that the TDP and fluid models are most nearly mutually applicable. The fluid model comes to equilibration faster than the TDP, as expected since the fluid model over predicts losses at long mean free paths. The time dependent densities computed with the MCS and TDP agree well. The time at which the densities equilibrate as computed with the MCS and TDP are shown in Fig. 4(b). The equilibration times for the MCS and TDP agree well over the full range of mean free paths investigated. Note that the equilibration time does not simply scale as the inverse of the pressure but rather reaches a lower limit due to the finite flight time of the particles. The deviation of the equilibration time from that one would expect from simple pressure scaling is also shown in Fig. 4(b). This deviation is indicated by τ/τ_p, where τ_p is the equilibration time based on continuum modeling. Significant deviation begins with $\lambda>2\Delta r$.

A final comparison was made between densities computed with the TDP and fluid methods, and the results are shown in Fig. 5. For this purpose we used the same geometry and conditions as described above but we used a distributed

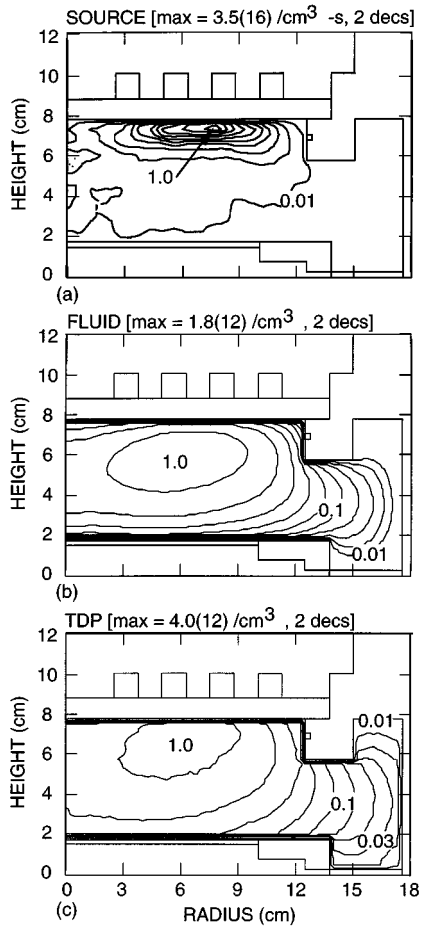

FIG. 5. Comparison of Ar* densities obtained from the fluid and TDP models for $\lambda=\Delta r$ using a distributed source. The quenching coefficient on walls is 0.5. (a) Ar* source function from the HPEM. (b) Ar* density obtained with the fluid model. (c) Ar* density obtained with the TDP. The contours are labeled with the fraction of the maximum value shown at the top of each figure.

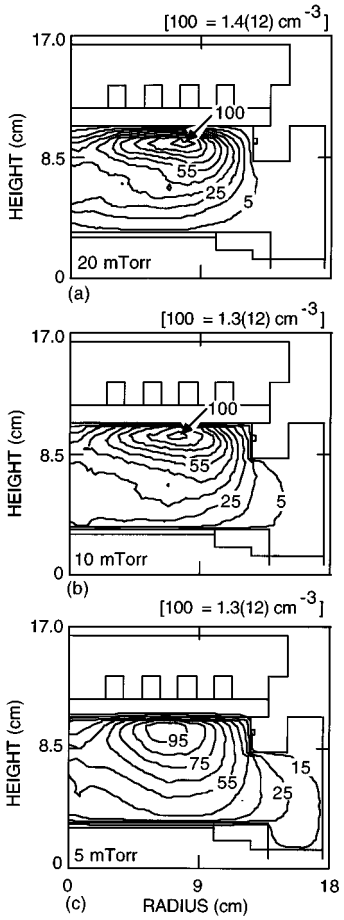

FIG. 6. Ar* densities in an ICP reactor obtained with the TDP being used as the neutral transport module in the HPEM for pressures of (a) 20, (b) 10, and (c) 5 mTorr. The contours are labeled with the percentage of the maximum value shown at the top of each figure. The source functions are similar to that shown in Fig. 5(a).

source of excited argon atoms, again nominally the Ar($4s$) state. This source function, shown in Fig. 5(a), was obtained from the HPEM for an ICP operating in 10 mTorr of Ar. The coil was driven at 13.56 MHz and produced a total inductively coupled power deposition of 500 W. The source function is maximum just under the dielectric at approximately half the radius. The source function has this shape because inductively coupled electric field is zero on the axis (by symmetry) and is zero on the metals outer walls. The skin depth for penetration of the electric field into the plasma is $\approx$1.5 cm, thereby accounting for the source being close to the window.[8]

A comparison of the excited neutral densities obtained with the TDP and the fluid model are shown in Figs. 5(b) and 5(c), respectively. The mean free path was chosen as $\lambda=0.25$ cm (equal to the mesh spacing) where the two methods are closest to being mutually valid, and the quenching coefficient on the walls is 0.5. The excited state density is maximum in an annular region corresponding to the maximum in the source function. Quenching on the walls produces steep gradients across the reactor. Both models predict similar density distributions, however the peak density predicted by the fluid model is lower than that of the TDP due to the over prediction of loses by the fluid model. Even though $\lambda\approx\Delta r$, there is evidence of long mean free path transport near the walls. The density gradient for the TDP is smaller than that for the fluid, a discrepancy which increases as either the mean free path or quenching coefficient increase.

Summarizing, the results from the TDP agree well with those from the MC simulation for both spatial and time dependencies for $\lambda>\Delta r$, thereby validating the TDP method. At smaller λ, the TDP appears not to be able to resolve the intracell collisions.

IV. TDP AS THE KINETIC MODULE IN THE HPEM

The TDP algorithms were employed as a long mean free path transport module in the HPEM. For demonstration purposes, we simulated Ar discharges using the geometry shown in Fig. 1. The species included in the model are Ar($3s$), Ar($4s$), Ar^+, and electrons. The reactions, rate coefficients and electron impact cross sections used in the HPEM are the same as discussed in Ref. 8. We examined ICP discharges operated at 5, 10, and 20 mTorr, corresponding to mean free paths of 1.577, 0.788, and 0.394 cm, respectively, based on a Lennard–Jones parameter of 3.54×10^{-8} cm. The quenching

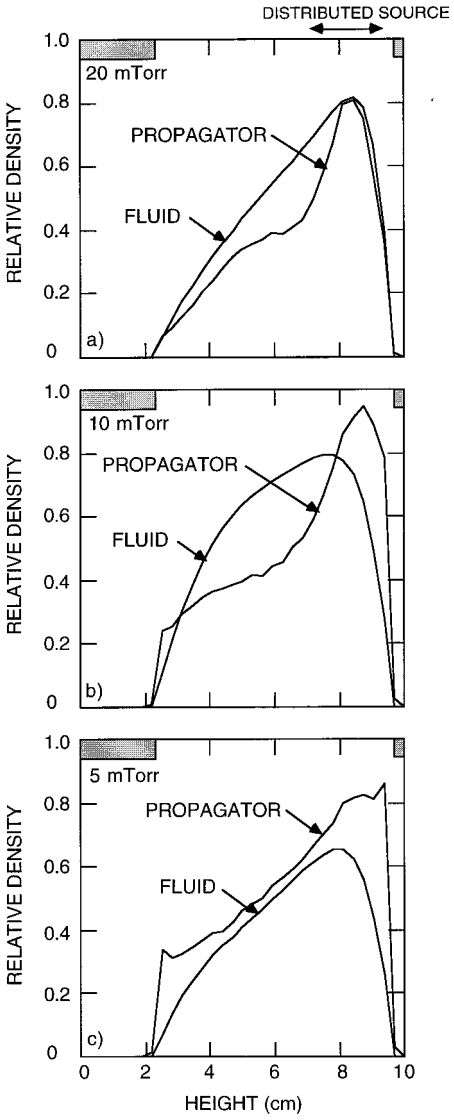

FIG. 7. Comparison of Ar* densities as a function of axial position obtained with TDP and fluid modules being used for the neutral transport module in the HPEM for pressures of (a) 20, (b) 10 and (c) 5 mTorr. The densities have been rescaled for purposes of comparison. The region over which the source function is large is shown at the top, and the boundaries of the substrate and window are shown in gray. At 20 mTorr, the flux at boundaries using the two methods are similar. Long mean free path effects are evident at 10 mTorr.

coefficient of Ar($4s$) on the walls of the discharge is unity. The ICP power is 500 W. The source function is similar to that shown in Fig. 5(a).

The densities of Ar* using the TDP method as the neutral transport module in the HPEM are shown in Fig. 6. Axial slices of the Ar* density at approximately the radius of the maximum density obtained using the TDP and a fluid module in the HPEM are shown in Fig. 7. The region over which the source is large is shown at the top of Fig. 7. The neutral transport transitions from continuum to long mean free path transport over this pressure range. At 20 mTorr, the Ar* densities using the TDP and fluid models are not significantly different in their spatial distributions. In particular, the maximum in the Ar* density occurs at approximately the same height above the substrate. The Ar* is largely confined to the region above the wafer near its source. At 10 mTorr, the peak of the Ar* density in the fluid has moved to a lower height whereas the peak Ar* density produced by the TDP method has remained nearer the window, and better reflects the source function by electron impact, while the Ar* extends further from the source at the periphery of the reactor. That trend continues at 5 mTorr. The boundary condition for the fluid equations is that excited state densities be zero at the wall. At 20 mTorr, this condition is well represented by the TDP. At 10 mTorr, this boundary condition at the substrate is marginal, whereas at the window the boundary condition is poor. This boundary condition is even less appropriate at 5 mTorr on the window. The close proximity of the Ar* source function to the window results in transport appearing to be more ballistic on the window side of the source. That is, the effective Knudson number for transport of Ar* from the source to the surface is larger on the window side of the source than on the substrate side, thereby making the continuum formulation less appropriate.

TABLE I. Memory requirements (MB) for the TDP method.

	$\lambda/\Delta r$				
IM	1	2	5	10	20
16	0.06	0.17	0.28	0.28	0.28
32	0.23	0.67	3.8	4.3	4.3
64	0.92	2.7	15.1	59.3	67.4
128	3.7	10.7	60.3	237	945

V. CONCLUDING REMARKS

A time dependent long mean free path transport method based on the use of a transition matrix (propagator) was demonstrated and applied to an ICP etching reactor geometry. Time dependence in the propagator method is obtained by storing a time history of past densities. These densities are then interpolated using a retarded time to account for the finite flight time of particles from their last collision to the present. The TDP method was compared to fluid and MC methods for test conditions. The TDP agreed well with the MC method when the particle mean free path exceeded a computational cell dimension. The TDP method agrees with uncorrected fluid calculations only for $\lambda=\Delta r$. In general, fluid calculations which are not flux limited are not valid for $\lambda>\Delta r$ and the TDP is not valid for $\lambda<\Delta r$. Fluid calculations for total particle inventory could be ''repaired'' by using an effective diffusion coefficient which is a function of the local diffusion length, but in general the spatial distribution of particle densities obtained by this method does not strictly agree with long mean free path techniques. Although the TDP method can be computationally faster compared to other long mean free path techniques, such as MCS, it does suffer from requiring large amounts of computer memory to store both the propagator and the time history of densities required by implementing a retarded time. A comparison of the computer requirements TDP and MCS methods is discussed in the Appendix. Far from the walls of reactors, the propagator depends only on the radial location in cylindrical

TABLE II. Memory requirements (MB) for the MCS method.

	ϵ			
IM	0.33	0.1	0.033	0.01
16	0.04	0.4	3.8	41
32	0.15	1.6	15.0	164
64	0.60	6.6	60.2	655
128	2.4	26.2	241	2.62 GB

geometries or is independent of position in Cartesian geometries. Therefore delineating such regions in the geometry of interest could save large amounts of memory.

ACKNOWLEDGMENTS

This work was supported by the National Science Foundation (ECS 94-04133, CTS94-12565). Semiconductor Research Corporation, Sandia National Laboratories/Sematech and the University of Wisconsin Engineering Research Center for Plasma Aided Manufacturing. The authors would like to thank Professor N. Hitchon for discussions on the propagator method.

APPENDIX: COMPARISON OF COMPUTER REQUIREMENTS FOR THE TDP AND MCS METHODS

The choice of which computational method one uses for long mean free path transport is often a function of the computer resources required for the task. In this appendix, we will estimate and compare the computing resources (memory and CPU time) required for the TDP and MCS methods. Since computing speeds vary between platforms, we make this comparison based on estimated floating point arithmetic operations (FLOP). We make the following assumptions.

(1) The numerical two-dimensional mesh is $IM \times IM$ cells.

(2) The ''horizon'' for computing and storing the propagator is 3λ, thereby requiring a propagator entry for $\pm(3\lambda/\Delta r)$ cells in each dimension for every ''launch point.''

(3) Incrementing the collision rate between any two cells using the TDP requires six FLOP.

(4) Advancing the equations of motions for the MCS requires eight FLOP. Recomputing velocities following a collision requires six FLOP.

(5) Single precision four byte words.

Storage requirements: Note that in estimating the memory necessary to store the propagator for the TDP, symmetries for the problem of choice can greatly reduce the memory requirements. For example, in a long cylinder, the propagator is a function only of radial position and not axial position, at least far from the ends of the cylinder. Therefore the same propagator can be used for nearly all axial locations. In this case, the memory requirements quoted below would be smaller by a factor of IM. In the absence of such symmetries, the storing the propagator requires

$$IM \times IM\{[2 \times \min(3\lambda/\Delta r, IM/2)]^2 + N_H\}$$

words of memory, where N_H is the number of past histories stored. These requirements in megabytes (MB) are shown in Table I for $N_H = 20$. The memory requirements for the MCS are a function of the tolerable error, ϵ. The number of MC particles scales as $1/\epsilon^2$. Assuming we maintain this error in each numerical cell, and that we maintain spatial and velocity components for each particle, the storage requirements are $IM \times IM \times 4(1/\epsilon^2)$ words of memory. These requirements in MB are shown in Table II. The MCS method requires lower memory only when reasonably large ϵ can be tolerated. In most MCS or PIC methods, however, this can be accomplished by using appropriate smoothing techniques.[16]

CPU requirements: Based on the cited estimates for FLOP per update, the operations per numerical cell for the TDP are

$$N_{\mathrm{TDP}} = \left[2\left(\frac{3\lambda}{\Delta r}\right)\right]^2 \times 6 .$$

Assuming we except a random error of ϵ for the MCS, the number of pseudoparticles/cell is $1/\epsilon^2$, and the operations per update (assuming three collisions within the horizon) is $N_{\mathrm{MCS}} = 1/\epsilon^2 \times 3 \times (8+6)$. The ratios of FLOPS between the TDP and MCS, $N_{\mathrm{TDP}}/N_{\mathrm{MCS}}$, are shown in Table III. The TDP is generally faster then the MCS when $\lambda/\Delta r$ is moderate and when reasonably fine precision is required for the MCS. Again, smoothing techniques may be used to reduce the number of MCS particles. For large values of $\lambda/\Delta r$ the TDP is slower due to the large number of cells within the transport ''horizon.''

TABLE III. Ratio of floating point operations $N_{\mathrm{TDP}}/N_{\mathrm{MCS}}$.

	ϵ			
$\lambda/\Delta r$	0.33	0.1	0.033	0.01
1	0.6	0.05	0.006	5×10^{-4}
2	2.2	0.2	0.022	0.002
5	14	1.3	0.14	0.013
10	56	5.1	5.6	0.051
20	222	20	2.2	0.2

[1] J. Hopwood, Plasma Sources Sci. Technol. **1**, 109 (1992).
[2] J. H. Keller, J. C. Forster, and M. S. Barnes, J. Vac. Sci. Technol. A **11**, 2487 (1993).
[3] M. S. Barnes, J. C. Forster, and J. H. Keller, Appl. Phys. Lett. **62**, 2622 (1993).
[4] R. Patrick, R. Schoenborn, and H. Toda, J. Vac. Sci. Technol. A **11**, 1296 (1993).
[5] J. B. Carter, J. P. Holland, E. Peltzer, B. Richardson, E. Bogle, H. T. Nguyen, Y. Melaku, D. Gates, and M. Ben-Dor, J. Vac. Sci. Technol. B **11**, 1301 (1993).
[6] J. Asmussen, in *Handbook of Plasma Processing Technology*, edited by S. M. Rossnagel, J. J. Cuomo, and W. D. Westwood (Noyes, Park Ridge, NJ, 1990), Chap. 11.
[7] D. J. Economou, T. J. Bartel, R. W. Wise, and D. P. Lymberopoulos, IEEE Trans. Plasma Sci. **23**, 581 (1995).
[8] P. L. G. Ventzek, M. Grapperhaus, and M. J. Kushner, V. Vac. Sci. Technol. B **12**, 1 (1994).
[9] R. J. Hoekstra and M. J. Kushner, J. Appl. Phys. **77**, 3668 (1995).
[10] V. Vahedi, C. K. Birsdall, M. A. Lieberman, G. DePeso, and T. D. Rognlien, Plasma Sources Sci. Technol. **2**, 273 (1993).
[11] R. E. P. Harvey, W. N. G. Hitchon, and G. J. Parker, J. Appl. Phys. **75**, 1940 (1994).
[12] R. E. P. Harvey, W. N. G. Hitchon, and G. J. Parker, IEEE Trans. Plasma Sci. **23**, 436 (1995).

[13] G. J. Parker, W. N. G. Hitchon, and J. E. Lawler, Phys. Lett. A **174**, 308 (1993).
[14] G. J. Parker, W. N. G. Hitchon, and J. E. Lawler, IEEE Trans. Plasma Sci. **21**, 228 (1993).
[15] See, e.g., E. S. Oran and J. P. Boris, *Numerical Simulation of Reactive Flows* (Elsevier, New York, 1987), Chap. 8.
[16] See, e.g., C. K. Birdsall and A. B. Langdon, *Plasma Physics via Computer Simulation* (McGraw–Hill, New York, 1985), Appendix C.